doi:10.3788/gzxb20164508.0806001

基于氮化钛薄膜表面等离子体共振特性的双芯光子晶体光纤温度传感器

白育堃[1,2],马颖[1],魏仁霄[1]

(1 天津理工大学 计算机与通信工程学院 通信器件与技术教育部工程研究中心,天津 300384)

(2 天津大学 精密仪器与光电子工程学院 激光与光电子研究所 光电信息科学技术教育部重点实验室,天津 300072)

摘 要:提出一种基于表面等离子体共振的双芯光子晶体光纤温度传感器,其中双芯光子晶体光纤为折射率导光型,其中心圆孔表面镀氮化钛薄膜,内部填充具有较大热敏系数的乙醇和氯仿的混合液体,其纤芯模与表面等离子体激元耦合的共振波长偏移可反映液体混合物的温度或折射率.利用全矢量有限元法分析了不同因素对传输损耗谱及其共振波长的影响.仿真结果表明:外包层空气孔直径增大,以及最内层包层空气孔直径和空气孔间距减小可以提高耦合效率,从而增强共振峰.对比分析发现在−20℃～120℃温度范围内,氮化钛薄膜比传统金膜表现出更好的等离子传感特性,随着膜厚增加,其共振波长偏移量增加,温度灵敏度提高,灵敏度最高可以达到 6.22 nm/K.

关键词:双芯光子晶体光纤;表面等离子体共振;全矢量有限元法;共振波长;氮化钛;温度传感

中图分类号:TP212 **文献标识码**:A **文章编号**:1004-4213(2016)08-0806001-5

A Dual-core Photonic Crystal Fiber Temperature Sensor Based on Surface Plasmon Resonance Characteristics of TiN

BAI Yu-kun[1,2], MA Ying[1], WEI Ren-xiao[1]

(1 *Engineering Research Center of Communication Devices and Technology, Ministry of Education, School of Computer and Communication Engineering, Tianjin University of Technology, Tianjin* 300384, *China*)

(2 *Key Laboratory of Optoelectronic Information Science and Technology, Ministry of Education, Institute of Laser and Optoelectronics, College of Precision Instrument and Optoelectronics Engineering, Tianjin University, Tianjin* 300072, *China*)

Abstract: A dual-core photonic crystal fiber temperature sensor based on the surface-plasmon-resonance was proposed. The holey analyte channel in the center of the index-guiding dual-core photonic crystal fiber is coated with a titanium nitride layer and filled with a liquid mixture of ethanol and chloroform exhibiting a large thermo-optic coefficient. The shift of the resonance wavelength for the coupling between the guided-core mode and surface-plasmon-polariton reflects the variation of temperature or refractive index of the infiltrated liquid mixture. With the full-vector finite element method, the impacts of various factors on the transmission loss spectrum and its resonance wavelength were analyzed. The numerical calculation indicates that by any of the means of increasing the outer-cladding-hole diameter and decreasing the innermost-cladding-hole diameter or the hole pitch, the coupling efficiency, namely the resonance amplitude, can be increased. It is found that titanium nitride film shows superior surface-plasmon-resonance sensing characteristics over conventional gold film in the temperature range of −20℃～120℃, featuring an increase of both resonance wavelength shift and temperature sensitivity

Foundation item: The National Natural Science Foundation of China (No. 11004152), the National Basic Research Program of China (No. 2010CB327801)

First author: BAI Yu-kun (1970−), male, associate professor, Ph. D. degree, mainly focuses on photonics and microwave technologies. Email: tjutbai_1@163.com

Received: Mar. 21, 2016; **Accepted**: May. 16, 2016

with an increase of film thickness and attaining the maximum temperature sensitivity of 6.22 nm/K.

Key words: Dual-core photonic crystal fiber; Surface plasmon resonance; Full-vector finite element method; Resonance wavelength; Titanium nitride; Temperature sensor

OCIS Codes: 060.5295; 310.6860;160.6840; 060.2390; 060.2370

0 Introduction

For the past few years, plasmonics has witnessed an enormous advance[1]. Conventional plasma materials mainly are gold and silver[2]. In recent years, researchers found a new plasmonic material, i. e. Titanium Nitride (TiN), in the visible and near Infrared (IR) region[3]. Despite of its optical losses which are similar to those of noble metals, it can be easily fabricated and integrated with standard silicon manufacturing processes[1,3]. Another key advantage of TiN is that the real part of its dielectric constant in the near-IR region is much smaller than that of noble metals[1,3].

Photonic Crystal Fiber (PCF), known as Microstructured Optical Fiber (MOF)[4], consists of an array of holes extending along the entire length of the fiber, and consequently exhibits a number of advantages for optical communication and sensing applications. PCF has a lot of peculiar properties, such as endless single-mode, high birefringence coefficient, controllable dispersion, high nonlinear coefficient, etc[5-8]. Song Xiao-li et al. designed a long-period PCF grating temperature sensor with a sensitivity of 1.766 nm/℃[9].

The PCF-based Surface Plasmon Resonance (SPR) technology has attracted continuous research interests. It is based on coupling the leaky guided-core mode to the plasmonic mode. In this context, the PCF-based SPR sensors which have the analyte infiltrated into the metal-coated holes of the PCF have been used for sensing[10-11]. Y. Peng et al. proposed a selectively coated photonic crystal fiber with a sensitivity of 0.72 nm/K [12]. Recently, Nan-Nan Luan et al. demonstrated a sensor design with a sensitivity of up to 5.6 nm/K [13].

In this paper, we propose a dual-core PCF temperature sensor based on the SPR properties of a new plasmonic material TiN in the near-infrared region. The proposed novel structure is easily implemented and can achieve a temperature sensitivity of up to 6.22 nm/K which is higher than that demonstrated so far.

1 Structure model

The schematic diagram of the dual-core-PCF SPR temperature sensor is shown in Fig. 1. This index-guiding dual-core PCF consists of five layers of air holes

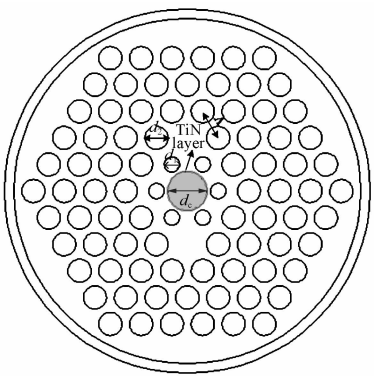

Fig. 1 Schematic diagram of the cross-section of the PCF-SPR temperature sensor

arranged in a regular hexagonal pattern. The surface of the void center hole is coated with TiN. Coating of TiN layer can be achieved by Chemical Vapor Deposition (CVD) technique[14-15]. And the center hole is filled with a large thermo-optic coefficient liquid. As shown in Fig. 1, the center hole is coated with a layer of TiN thin film with thickness $t_s=50$ nm. The diameter of the center hole is $d_c=2\mu$m, while it is $d_1=0.8$ μm for the holes in the innermost layer, and $d_2=1.2$ μm for the other air holes. The pitch of the underlying hexagonal lattice is $\Lambda=1.6$ μm. The Refractive Index (RI) of the PCF material is assumed to be 1.45 (fused silica), and the permittivity of TiN ε_m is given by the Drude model[16] as

$$\varepsilon_m(\omega)=\varepsilon_\infty-\frac{\omega_p^2}{\omega^2+i\omega\Gamma} \tag{1}$$

where ε_∞ is due to the screening effect of bound electrons in the material and can be considered as a constant in the frequency band of interest, $\varepsilon_\infty=2.599$[16] in the near-infrared region. Where Γ is the damping coefficient of free carriers or the Drude-relaxation rate, ω_p is the plasma frequency as

$$\omega_p=\sqrt{\frac{ne^2}{\mu\varepsilon_0}} \tag{2}$$

where n is the carrier concentration, e is electron charge, μ is effective mass of TiN, ε_0 is permittivity of vacuum.

The refractive index of the liquid mixture in the analyte channel can be evaluated by [5]

$$n=x\%\times[n_{\text{chloroform}}|_{T=293K}+\mathrm{d}n_{\text{chloroform}}/\mathrm{d}T\times(T-293)]+(100-x)\%\times[n_{\text{ethanol}}|_{T=293K}+\mathrm{d}n_{\text{ethanol}}/\mathrm{d}T\times(T-293)] \tag{3}$$

where $x\%$ is the mass ratio of chloroform and $(100-x)\%$ is that of ethanol, the thermo-optic coefficients of chloroform and ethanol are -6.328×10^{-4}/K and

-3.94×10^{-4}/K respectively, n is the refractive indices at temperature T[5]. The refractive indexes of $n_{ethanol}$ and $n_{chloroform}$ are defined as 1.36 and 1.44 at $T=293$ K respectively. Compared with the liquid mixture, the thermo-optic coefficient of silica (8.6×10^{-6}/K) is smaller by two orders of magnitude. Therefore, we set the refractive index of fused silica as a constant. The ratio of chloroform and ethanol is defined as 5∶5. The relationship of refractive indexes of mixed liquid and the background material of PCF with the increase of temperature are shown in Fig. 2. As seen in the figure, the refractive index of mixed liquid decreases, and the refractive index of fused silica is practically constant with an increase of temperature.

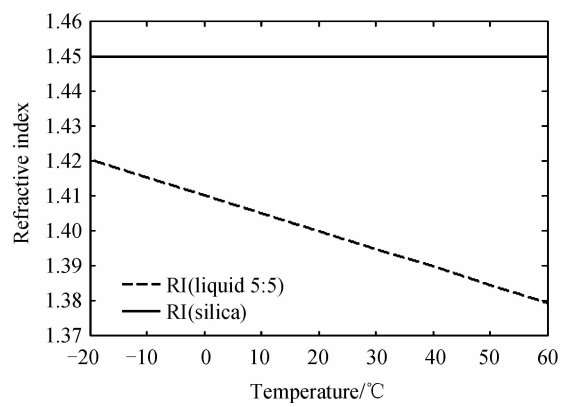

Fig. 2 Temperature dependence of refractive indexes of the liquid mixture and fused silica

2 Numerical analysis

In this paper, the full-vector finite element method[17-19] based software package COMSOL Multiphysics is used as the simulation tool. The parameters of the structure are $d_c=2$ μm, $d_1=0.8$ μm, $d_2=1.2$ μm, $\Lambda=1.6$ μm. When it comes to the change of one parameter, other parameters still keep the above values. The electric field distribution of fundamental modes and the three dimensional energy distribution are shown in Fig. 3 (a) and (b) respectively. As shown in the figures, the electric field direction is designated by the arrows and all the energy is concentrated in the two cores.

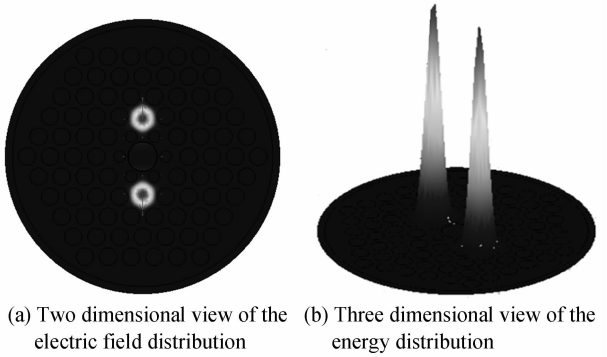

Fig. 3 The electric field distribution and the energy distribution of the fundamental mode

The energy is largely concentrated in the dual-core areas of the PCF, and others penetrate into the TiN to excite the plasmonic mode and the energy of the guided-core mode suffers from attenuation. It is very important to get loss spectrum of the temperature sensor. As various wavelengths of light are incident, the attenuation constant of the fundamental mode is calculated. When the phase matching is satisfied, the energy of a guided-core mode is efficiently transferred to plasmonic mode[13]. A peak of the loss spectrum will be formed at this wavelength. The attenuation constant α is proportional to the imaginary part of the effective index (n_{eff}) according to the relation as follows

$$\alpha=2k_0\,\mathrm{Im}[n_{eff}] \tag{4}$$

where, $k_0=2\pi/\lambda$is the free-space wave number of free space. The optical fiber transmission loss α_{loss} can be expressed with the attenuation constant α as [5]

$$\alpha_{loss}=10\lg e\cdot\alpha \tag{5}$$

From Eqs. (4) and (5), the expression of the optical fiber transmission loss is

$$\alpha_{loss}=10\lg e\cdot 2k_0\,\mathrm{Im}[n_{eff}]=8.686\cdot k_0\,\mathrm{Im}[n_{eff}]\ (\mathrm{dB/m}) \tag{6}$$

The imaginary part of the guided-core-mode effective refractive index will change acutely due to the plasmon resonance between the guided-core mode and the plasmonic mode. Fig. 4 shows the calculated loss spectra of the guided-core modes in the wavelength range of 0.81～1.05 μm when the RI of the liquid is 1.4. As shown in Fig. 4, the plasmonic excitation peak located at the wavelength of 0.92 μm is defined by an increase in the guided-core mode propagation losses. When the energy is transferred into the lossy plasmonic mode, the losses of the guided-core mode increase dramatically. The electric field distribution of the guided-core modes in one of the two index-guiding cores

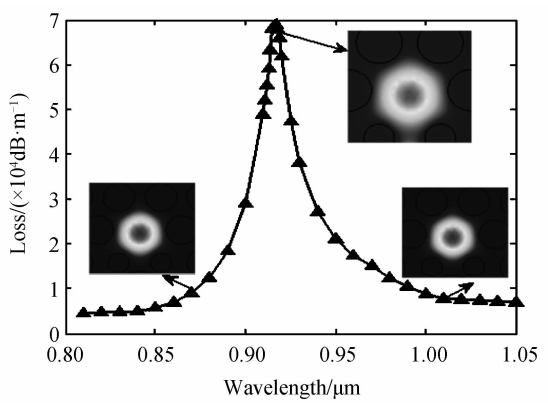

Fig. 4 Loss spectra of the SPR sensor when the refractive index of the liquid is 1.4 and the TiN thickness is 60 nm. Insets show the electric field distributions of the guided-core modes

(insets in Fig. 4) is clearly shown. At resonance wavelengths (phase-matching wavelengths), the energy of the guided-core modes is transmitted to that of the plasmonic mode. Thus, it is obvious that there is a peak of the loss spectrum at this wavelength. At nonresonance wavelengths, most of the energy is confined in the core area. The electric field distributions of the two cores are identical.

The temperature sensitivity is

$$S_\lambda[\mathrm{nm/K}]=\Delta\lambda_{\mathrm{peak}}/\Delta T \tag{7}$$

The influence of the fiber geometry on the sensing performance is shown in Figs. 5, 6 and 7. We choose $t_s=50$ nm and the refractive index of the liquid is 1.39. Fig. 5 shows the d_1-dependent loss properties. With the decrease of d_1, the peak of loss spectrum becomes more obvious because of the higher coupling efficiency between the guided-core mode and plasmonic mode.

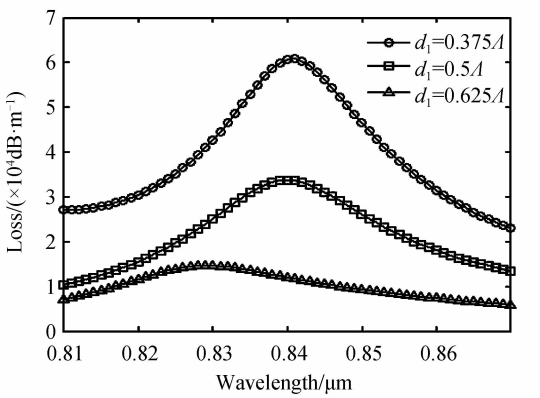

Fig. 5 Loss spectra of the SPR sensor with different values of d_1

Fig. 6 shows that d_2 is varied from 0.65Λ to 0.75Λ while keeping all other structural parameters constant. The increase of d_2 leads to a red shift of the resonance wavelength. Furthermore, the loss value is increased at the same wavelength with the increase of d_2.

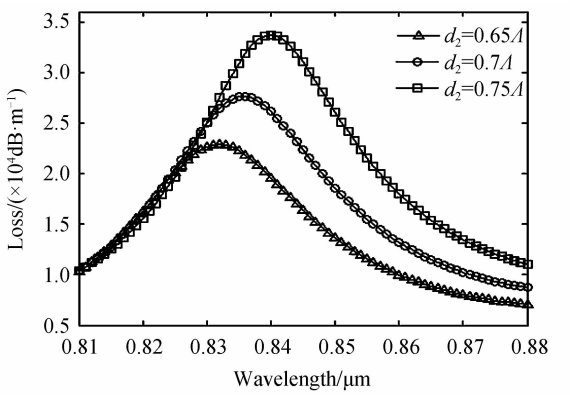

Fig. 6 Loss spectra of the SPR sensor with different values of d_2

Fig. 7 shows the Λ-dependent loss properties. It shows that the peak of loss spectrum tend to be flat with the increase of Λ. Furthermore, it is also seen that the sensitivity for $\Lambda=1.6$ μm is better than that for the other Λ values.

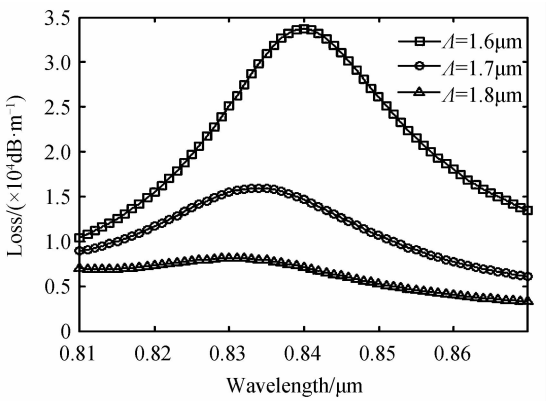

Fig. 7 Loss spectra of the SPR sensor with different values of Λ

For different TiN thicknesses, we calculated the surface plasmon resonance wavelength variation within the temperature range of −20℃ ~ 40℃. Fig. 8 shows the change of resonance wavelength for the TiN thicknesses of 40 nm, 50 nm, and 60 nm. We can find that the plasmonic peak shifts to a longer wavelength and displays a sharper variation slope when the thickness of the TiN coating is increased.

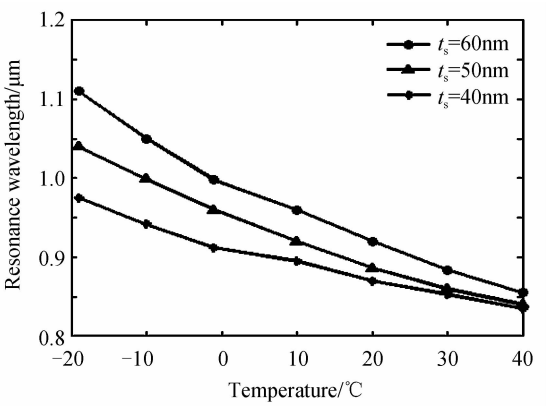

Fig. 8 Resonance wavelength versus temperature curves with the TiN thicknesses of 40 nm, 50nm and 60 nm

As a set of ideal parameters, $d_1=0.8$ μm, $d_2=1.2$ μm, $d_c=2$ μm, $\Lambda=1.6$ μm and $t_s=60$ nm are used in the following calculations.

Fig. 9 shows the resonance wavelength variation of the SPR sensor within an extended temperature range of −20℃ ~ 140℃. We can find that the drop of temperature leads to a red shift of resonance wavelength.

Compared with conventional plasma material such as Au, TiN has better plasmonic performance in the near-infrared region. In Fig. 9, the resonance wavelengths of the TiN layer and Au layer of the same thickness are compared within the same temperature range. It is shown that the resonance wavelengths of the two layers are different at the same temperature due to their different dielectric constants.

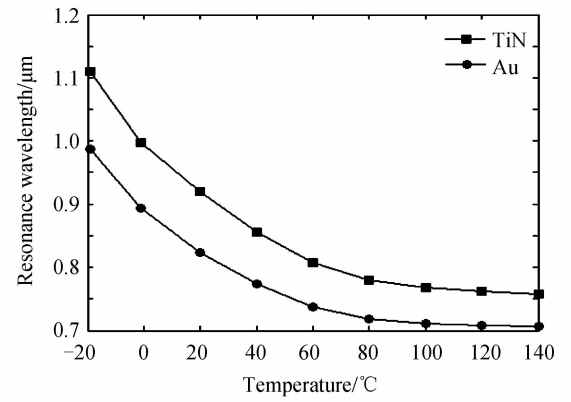

Fig. 9 Resonance wavelength curves for the coatings of TiN layer and Au layer with the same thickness of 60 nm

Calculated by Eq. (7), the corresponding sensitivity curves are shown in Fig. 10. As seen in the figure, sensitivity up to 6.22 nm/K of the TiN film in the temperature range of −19℃ ~ −1℃ is achieved. We can also conclude that the sensitivity of the TiN layer is higher than that of Au layer in the extended temperature range.

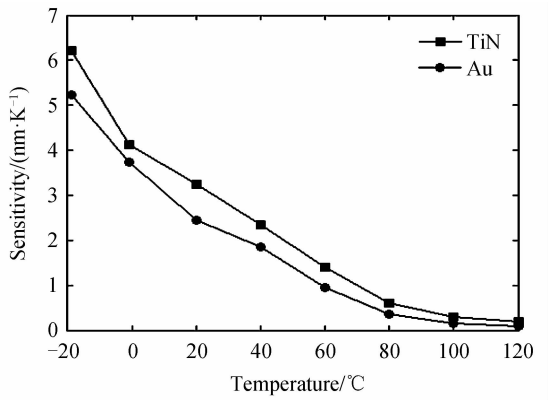

Fig. 10 Sensitivity curves for the coatings of TiN layer and Au layer with the same thickness of 60 nm

3 Conclusion

In this paper we have analyzed a surface plasmon resonance temperature sensor based on PCF filled with a liquid mixture with high thermo-optic coefficient. The coupling efficiency between the guided-core mode and the plasmonic mode is affected by the refractive index or temperature of the infiltrated liquid mixture. TiN in the proposed design exhibits superior plasmonic performance than conventional noble metal Au in the near-infrared region. The implementation of the PCF-SPR sensor is quite simple, and a high temperature sensitivity can be achieved.

References

[1] NAIK G V, SCHROEDER J L, NI X, *et al*. Titanium nitride as a plasmonic material for visible and near-infrared wavelengths[J]. *Optical Materials Express*, 2012, **2**(4): 478-489.

[2] BOLTASSEVA A, ATWATER H A. Low-loss plasmonic metamaterials[J]. *Science*, 2011, **21**(1): 290-291.

[3] NAIK G V, KIM J, BOLTASSEVA A. Oxides and nitrides as alternative plasmonic materials in the optical range[J]. *Optical Materials Express*, 2011, **1**(6): 1090-1099.

[4] ZHU Hong-tao, LOU Qi-hong, ZHOU Jun, *et al*. Theoretical study on the heat dissipation ability of double-cladding photonic crystal fiber[J]. *Acta Photonica Sinica*, 2009, **38**(1):60-63.

[5] WANG Min-tuo, LU Ying, HAO Cong-jing, *et al*. Simulation analysis of a temperature sensor based on photonic crystal fiber filled with different shapes of nanowires[J]. *Optik*, 2015, **126**(23): 3687-3691.

[6] ZHANG Pei-pei, YAO Jian-quan, CUI Hai-xia, *et al*. A surface plasmon resonance sensor based on a multi-core photonic crystal fiber[J]. *Optoelectronics Letters*, 2013, **9**(5):0342.

[7] BING P B, LI Z Y, YAO J Q, *et al*. A photonic crystal fiber based on surface Plasmon resonance temperature sensor with liquid core[J]. *Modern Physics Letters B*, 2012, **26**(13): 1250082.

[8] QIN Wei, LI Shu-guang, XUE Jian-rong, *et al*. Numerical analysis of a photonic crystal fiber based on two polarized modes for biosensing applications[J]. *Chinese Physics B*, 2013, **22**(7): 074213.

[9] SONG Xiao-li, BAI Yu-kun, REN Guang-jun, *et al*. Analysis of temperature sensing characteristics of a long-period grating formed in a liquid-filled photonic crystal fiber[J]. *Chinese Journal of Lasers*, 2011, **38**(12): 1205007.

[10] DASH J N, JHA R. SPR biosensor based on polymer PCF coated with conducting metal oxide[J]. *IEEE Photonics Technology Letters*, 2014, **26**(6): 595-598.

[11] AKOWUAH T K, GORMAN T, ADEMGIL H, *et al*. Numerical analysis of a photonic crystal fiber for biosensing applications[J]. *IEEE Journal of Quantum Electronics*, 2012, **48**(11): 1403-1410.

[12] PENG Y. Temperature sensor based on surface plasmon resonance within selectively coated photonic crystal fiber[J]. *Applied Optics*, 2012, **51**(26): 6361-6367.

[13] LUAN Nan-nan, WANG Ran, LU Ying, *et al*. Simulation of surface plasmon resonance temperature sensor based on liquid mixture-filling microstructured optical fiber[J]. *Optical Engineering*, 2014, **53**(6): 067103.

[14] CHENG H E, LEE W J. Properties of TiN films grown by atomic-layer chemical vapor deposition with a modified gaseous-pulse sequence[J]. *Materials Chemistry and Physics*, 2006, **97**(2-3): 315-320.

[15] SAKAMOTO T, SHIMADA S, KIYONO H, *et al*. Water vapor-controlled thermal plasma chemical vapor deposition of double-layered TiN/PSZ coatings on Si and WC-Co substrates [J]. *Materials Science and Engineering B*, 2010, **172**(2): 201-206.

[16] KANG J H, KIM J K. Structural, optical, and electronic properties of cubic TiN_x compounds[J]. *Journal of Applied Physics*, 1999, **86**(1): 346-350.

[17] HE Ru-shuang, ZHANG Bin, WANG Zhen-yu, *et al*. A polymer dispersed liquid crystal Fresnel zone plate[J]. *Acta Photonica Sinica*, 2014, **43**(9): 0923003.

[18] GUO Shi-liang, HU Chun-hai, HUANG Hui, *et al*. Analysis of coupling characteristics of dual-core photonic crystal fiber based on tellurite glass[J]. *Acta Photonica Sinica*, 2015, **44**(1): 0106001.

[19] YAO Hong-bing, YU Wen-long, YANG Zhao, *et al*. Numerical simulation of AZ31B magnesium alloy shocked with Femtosecond laser[J]. *Acta Photonica Sinica*, 2015, **44**(4): 0414002.